Nuclear Inst. and Methods in Physics Research, A 985 (2021) 164679

Contents lists available at ScienceDirect

Nuclear Inst. and Methods in Physics Research, A

journal homepage: www.elsevier.com/locate/nima

The performance of the commissioned Notre Dame multi-reflection time-of-flight mass spectrometer

B. Liu *, M. Brodeur, D.P. Burdette, J.M. Kelly, T. Kim, J. Long, P.D. O'Malley

Department of Physics, University of Notre Dame, Notre Dame, IN 46556, USA

ARTICLE INFO

Keywords:
Multi-reflection time-of-flight mass spectrometer
Isobar separator
Ion trap
Radioactive ion beams

ABSTRACT

The future $N = 126$ factory at Argonne National Laboratory is aimed to produce neutron-rich elements around the $N = 126$ peak of the rapid-neutron capture process using multi-nucleon transfer reactions. However, this radioactive ion beam production method will entail the delivery of contaminant ions. To remove the isobar contaminants from the beam, a multi-reflection time-of-flight mass spectrometer has been built and successfully commissioned at the University of Notre Dame, reaching a resolving power of 70,000, with an efficiency of 10%. According to stability study conducted, the resolving power is potentially limited to 83,000 by the power supply stability, however it can be mitigated by the addition of RC filtration as done for other MR-TOFs. The commissioned MR-TOF has been transported to Argonne National Laboratory to be used in the $N = 126$ factory.

1. Introduction

The rapid neutron capture process (r-process) is responsible for the production of almost half of the stable and some long-lived radioactive elements heavier than iron [1]. More experimental data are needed to enable the study of the r-process abundance. The abundance pattern is especially sensitive to the properties of nuclei near the $N = 82$ and $N = 126$ shell closures [2]. Experimental data near the latter is especially sparse due to the difficulty in producing neutron-rich nuclei near $N = 126$. The $N = 126$ factory, under construction at Argonne National Laboratory [3], aims to remedy this lack of data by employing multi-nucleon transfer reactions as a means to produce neutron rich isotopes. The radioactive ion beam (RIB) produced will however contain many contaminants. These contaminants will be cleaned first by a mass analyzing magnet to remove non-isobars ($M/\Delta M \approx 1500$) and then by a multi-reflection time-of-flight mass spectrometer (MR-TOF) to remove isobars ($M/\Delta M \approx 100,000$) [3,4]. The construction [5] and commissioning of this MR-TOF was done using an off-line setup [4] at the University of Notre Dame. This paper reports on the final off-line commissioning results, including the optimization methods used, resolving power and efficiency results as well as the stability performance of the MR-TOF, before it was shipped to Argonne National Laboratory.

2. The MR-TOF off-line setup

Fig. 1 shows the experimental setup used for this work with the main components marked out. In the off-line setup, a heated alkali source [6] followed by an anode produces a continuous cocktail beam. Then a Bradbury–Nielsen gate (BNG) [7] is used to bunch the beam with a 160 ns opening time [4]. After going through steering and focusing ion optical elements, the ion bunch enters the MR-TOF and is captured using the in-trap lift methods [8]. After a certain number of cycles, the bunches are released and hit a microchannel plate detector (MCP) placed at the end of the beam line to record their time-of-flight.

As Fig. 2 shows, the MR-TOF contains two electrostatic mirrors comprised of five pairs of mirror electrodes, one pair of lens and a drift tube (DT) located between the lens. The paired mirrors and lens create a symmetric electric potential barrier on both sides of the DT as indicated in Fig. 2. Thus just by lowering or raising the DT potential when an ion bunch is at the middle of the DT, ions can be captured or released by the MR-TOF. A Model DG535 digital pulse generator [9] is used to trigger the BNG and the DT switch. This pulser is also used to trigger the start of the data acquisition by a SR430 multi-channel scaler [10]. The detailed circuit diagram is shown in Fig. 3.

The details of the MR-TOF structure design can be found in [5] and the detailed off-line setup can be found in [4]. There were a few changes made compared to the setup in [4]. Firstly, the K ion source was replaced by Rb. The species from that source can be found in the time-of-flight spectrum of Fig. 4. The dominant isotopes are ^{85}Rb and ^{87}Rb with natural abundances. Secondly, to improve the quality of the beam, a pair of 2 mm diameter apertures were added on either side of the BNG. This change aimed to reduce the emittance by limiting the radial spread of the beam. Finally, the MCP and Faraday cup (FC) before the MR-TOF were removed due to grounding and misalignment issues that resulted in beam loss.

* Corresponding author.
E-mail address: bliu4@nd.edu (B. Liu).

https://doi.org/10.1016/j.nima.2020.164679
Received 31 July 2020; Received in revised form 11 September 2020; Accepted 18 September 2020
Available online 23 September 2020
0168-9002/

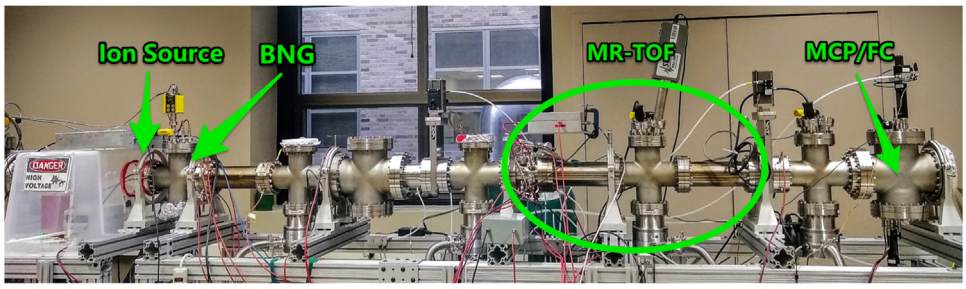

Fig. 1. Photo of the off-line commissioning beam line at the University of Notre Dame. Indicated are the location of the ion source, Bradbury–Nielsen gate (BNG), MR-TOF and MCP.

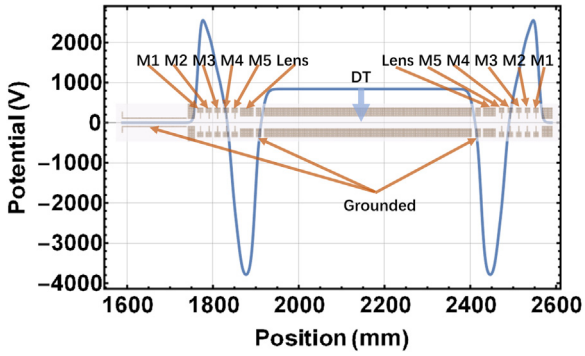

Fig. 2. The MR-TOF electrode structure with the ideal potential.

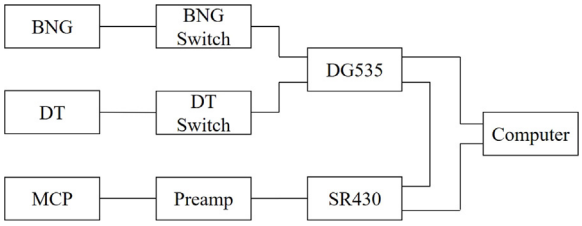

Fig. 3. Circuit diagram of the MR-TOF off-line commissioning beam line.

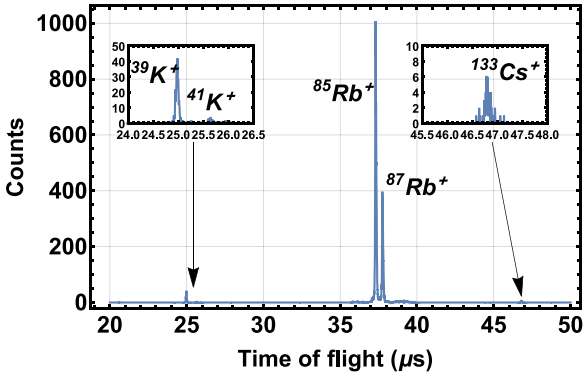

Fig. 4. Time-of-flight spectrum indicating the various isotopes present in the Rb ion source. The counts were recorded on the MCP after the MR-TOF. For this measurement, the bunch was shot through the MR-TOF.

3. Optimization of the MR-TOF

The goal of the optimization process is to find the electrode potentials that maximize both the efficiency and the resolving power. The efficiency is defined as the ratio of the total number of counts after a certain number of loops in the MR-TOF to the total number of counts

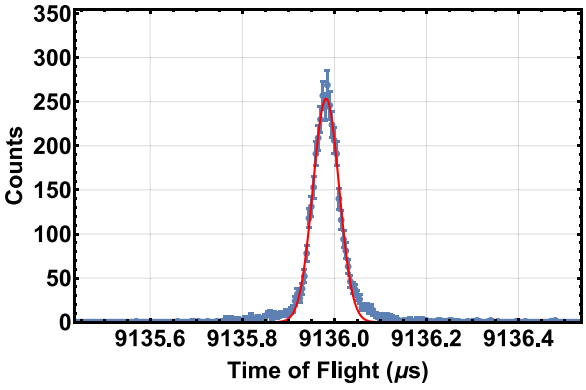

Fig. 5. A typical time-of-flight spectrum with Gaussian fit.

obtained when shooting through the MR-TOF. The resolving power is defined as $R = T/(2\Delta T)$, where T is the total time-of-flight and ΔT is the full width at half maximum (FWHM) of the bunch. The total time-of-flight is the sum of the time taken to reach the DT from the BNG, the time spent in the MR-TOF and the time-of-flight to the MCP upon extraction.

Due to the bunching method and the 2 mm diameter apertures, most of the ions produced by the ion source are not getting to the MR-TOF. Typically, we have about 0.25–0.5 ion per shot. As such, we need to typically record 4000–8000 shots in order to have sufficient statistics to have a fittable time-of-flight spectrum. As more ions are accumulated, a Gaussian shaped peak is obtained.

To determine if a given setting is optimal, the main quantities studied are the total number of counts, the height, the FWHM of the peak and its symmetry. Fig. 5 shows a typical peak with the Gaussian fit. The presence of longer exponential-shaped tails is noticeable. These can be caused by a spherical aberration, an imperfection in the trap potential, or a mechanical misalignment. While a Gaussian fit is adequate for our off-line-commissioning, high-precision mass measurements would require the use of more elaborated fit functions with asymmetric exponential tails such as the Hyper-EMG family of functions [11].

A LabVIEW code has been written to scan over a given voltage range for one or two given electrodes and a Mathematica code has been written to analyze the data and plot the results to help determine the optimal voltage(s) applied to the electrode(s). Fig. 6 shows an example of a two dimension FWHM contour plot when varying mirror 1 (M1) and mirror 2 (M2). In this case, the smallest FWHM located at M1 = 2832.5 V and M2 = 2155 V is the potential optimal choice. After checking the contour plots of the other quantities, which showed agreement with these two values, we adopted them as our optimal voltages for M1 and M2. During the whole optimization process, we followed a linear progression through electrodes as M1 vs. M2, M2 vs. M3, M3 vs. M4, etc. A previously optimized electrode was always

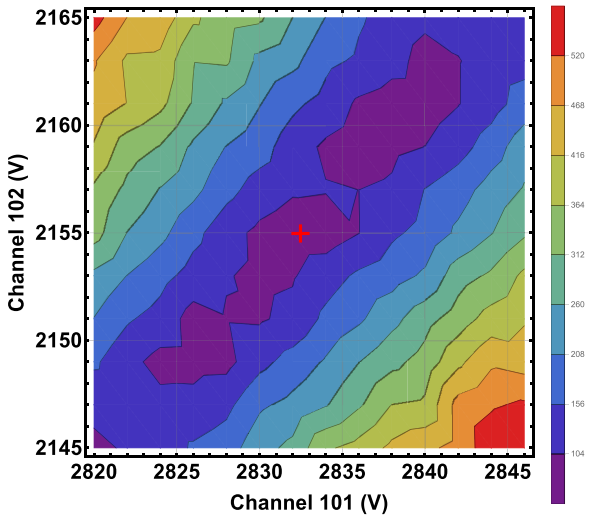

Fig. 6. 2 dimensional contour plot of the FWHM of the time-of-flight spectra as a function of the M1 and M2 electrode potentials. The optimal choice for M1 and M2 is indicated by the red cross.

repeated to ensure it has an optimal potential. The procedure was repeated as needed. The electric potential along the axis of the MR-TOF created by the optimized potential on each electrodes given in Table 1 is shown in Fig. 2. Note the optimization was based on 400 loops.

After the optimization procedure, we reached the efficiency and resolving power shown in Fig. 7. As the figure indicates, the resolving power and the efficiency are both functions of number of loops in the MR-TOF. The resolving power increases as the number of loops increases until about 250 loops and then reaches a plateau around 70,000. The efficiency plot shows that most ions are lost in the first 5 to 10 loops and the remaining ions tend to stay in the MR-TOF for the remaining number of loops. At 400 loops, we still have an efficiency around 10%. The efficiency curve can be fitted by a function with two exponential decay components and a constant, which gives two lifetimes of 15(3) μs and 1.9(4) ms respectively. This illustrates that there are two distinct loss mechanisms. The quick loss could be due to the acceptance of the MR-TOF, the emittance of the beam or a mechanical misalignment. The collision with residual gas inside the chamber could cause the slow loss. Note that because ^{87}Rb was also being injected in the MR-TOF together with ^{85}Rb, it is possible that it could appear near ^{85}Rb after a certain number of loop. Loop 85 and loop 690 are cases where ^{87}Rb happens to be overlapping with the ^{85}Rb peak we were fitting resulting in its broadening and the large changes in both efficiency and the resolving power.

We then studied the symmetry of the time-of-flight distribution by taking 940 spectra at 400 loops, re-centering them to correct for temporal drifts (see Section 4) and then adding them together, resulting in the sum peak of Fig. 8. As it shows, the peak is symmetric, except for a small bump on the left side visible in log-scale. That could be the result of having a non-ideal trapping potential.

4. Stability of the MR-TOF

The ultimate resolving power of a MR-TOF and its ability to perform a precise and accurate mass measurement will depend on the temporal stability of the time-of-flight spectra. Such stability will primarily be affected by the voltage output of the power supplies, which can be affected by variations in the room temperature. Thus the temporal stability of the time-of-flight spectra together with the power supply outputs and the temperature were monitored. The time-of-flight temporal stability was studied in terms of the position of the peak centroid and the width of the peak. The influence of the power supply on these two aspects were also calculated quantitatively.

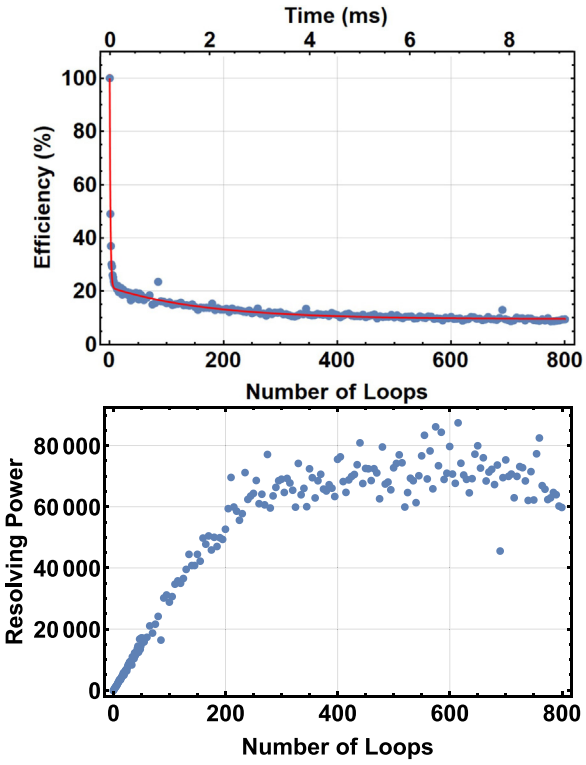

Fig. 7. Transfer efficiency (top panel) as a function of number of loops and as a function of time-of-flight. Mass resolving power (bottom panel) as a function of number of loops.

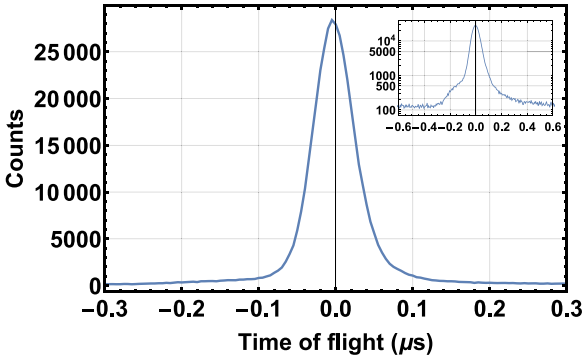

Fig. 8. The sum peak of 940 re-centered peaks and the sum peak where the *y*-axis is in log-scale (top right corner).

4.1. Temporal stability monitoring

To study the time-of-flight temporal stability, the spectra were recorded repeatedly over a certain amount of time. Considering the stability of the power supplies could potentially impact the MR-TOF's performance significantly and the temperature fluctuation in the room may also have an impact on the stability of the power supply or on the time-of-flight, we monitored both the voltage of the power supply and the temperature together with the spectra information as a function of time.

In this monitoring process, a CADDOCK HVD5-A50M-050-05 1909 ultra-precision voltage divider [12] was used to decrease the high voltage output by a factor of 1000, and then the voltages were measured by a voltmeter which has a resolution of 1 μV. Three temperature sensors were attached with one to the beam line near the ion source, one at the location of the MR-TOF DT, and one at the end of the beam line.

Table 1
Optimized electrode potentials for a 3 keV ion beam, fitted slopes of the time-of-flight variation with applied potential (Fig. 9), standard deviation of the peak centroid variation σ_{TOF}, standard deviation of the peak distribution σ_{spec}, the voltage variation standard deviation σ'_V and its contribution to the peak position variation σ'_{TOF}, the voltage fluctuation standard deviation σ''_V and its contribution to the peak width σ'_{spec}.

Electrode	Potential (V)	Slope (ns/V)	σ_{TOF} (ns)	σ_{spec} (ns)	σ'_V (V)	σ'_{TOF} (ns)	σ''_V (V)	σ'_{spec} (ns)
M1	2837	−483(1)	88	53.69(3)	0.021	10	0.019	9.0
M2	2159	−1617(7)	62	58.63(3)	0.013	21	0.013	21
M3	1200	493(1)	34	58.82(2)	0.0054	2.7	0.0076	3.7
M4	240	122.2(5)	25	57.94(3)	0.0021	0.26	0.0051	0.63
M5	−2340	−42.6(1)	71	56.79(3)	0.017	0.74	0.019	0.81
Lens[a]	−3925	−56.1(2)	81	56.54(3)				
DT	841	2(1)	100	60.01(3)	0.22	0.45	0.44	0.88
			66[b]	57.42(1)[c]		24[d]		23[d]

[a]The voltage of the lens has not been monitored.
[b]Mean.
[c]Weighted average.
[d]Added in quadrature.

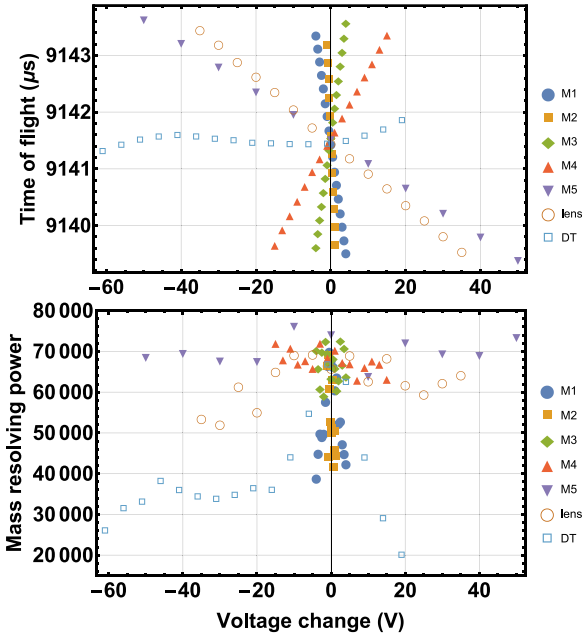

Fig. 9. The change of time-of-flight (top panel) and resolving power (bottom panel) varying different electrode voltages.

The temperatures were measured by three 1-wire digital thermometers (Model DS18B20) [13] with a resolution of 0.06°C. To monitor the temperature fluctuation during the whole day, we recorded at least 24 h for each electrodes (five mirrors, the lens and the DT). Each data point contains 8000 shots.

The monitoring was repeated because we were only able to monitor one electrode at a time. Fig. 10 shows the results of the two most sensitive electrodes, M1 and M2. While a certain correlation between TOF and temperature seems to be present in the first 5 h, it vanishes afterwards. Also, while a certain correlation covering the time span between temperature and power supply output can be seen for M2, such long-term correlation is not obviously present for M1. Hence, the plots from Fig. 10 and the behavior of other electrodes all indicate there is no consistent systematic correlation covering long time span between the time-of-flight, temperature, or the voltage on each electrode.

The monitored spectrum quantities are listed quantitatively in Table 1, including the standard deviation of the peak centroid variation σ_{TOF} and the mean value of the standard deviation of the peak distribution σ_{spec} over the ∼24 h recording period for a given electrode. σ_{TOF} tells us how much the position of the peak moves and σ_{spec} shows how much the peak spread in terms of its width. The typical σ_{TOF}, taken as the average of the results for each electrode scan, is 66 ns, while σ_{spec} is on average 57 ns. It should be noted that during the stability studies the tune of the MR-TOF was not optimal.

4.2. Power supply influence on the stability

The power supply stability can both impact the position and the width of the peak. The long term variation of the power supplies affects the peak position and the quick fluctuation of the voltage affects the peak width.

4.2.1. Time-of-flight sensitivity to electrode potential

The time-of-flight sensitivity to electrode potential can be studied by varying the potentials on each electrode. Fig. 9 shows how the time-of-flight of the bunch and the resolving power change when varying the voltages on each electrode. It shows that the time-of-flight is very sensitive to changes in the potential of electrodes M1, M2 and M3 since a small change in the potential results in a big change of the time-of-flight and a rapid decrease of the resolving power, while the other electrodes are less sensitive and have a relatively smaller impact. The sensitivity of the time-of-flight to the applied potential was determined quantitatively through a linear regression of the data resulting in the slope listed in Table 1.

4.2.2. Power supply influence on the position of the time-of-flight spectra

The voltage stability is one of the factors impacting the time-of-flight stability, resulting in the 66 ns standard deviation of the time-of-flight variation shown in Fig. 10. To see how much the variation of voltages contributes to the peak position variation, we took a 19 point moving average of the voltage (see the bottom panels in Fig. 10) and calculated its standard deviation σ'_V. In this way, we removed the influence of quick voltage fluctuation and revealed the voltage variation trend. The product of the slope and the corresponding σ'_V in Table 1 is the contribution to the peak position variation σ'_{TOF} from a given electrode's power supply variation. By adding the different σ'_{TOF} in quadrature, we got an estimate of the contribution to the peak position variation from all the electrodes inside the MR-TOF except for the lens, whose contribution will be negligible, of around 24 ns. The variation of the voltages cannot account for the 66 ns variation seen. One other factor is the DG535 pulse generator 25 ppm time base error. Hence, the 9059 μs time delay (at 400 loops) that the DG535 introduces between the capture and extraction of the bunch can potentially introduce a variation of 226 ns in the time base, which could be the other source of the peak position variation.

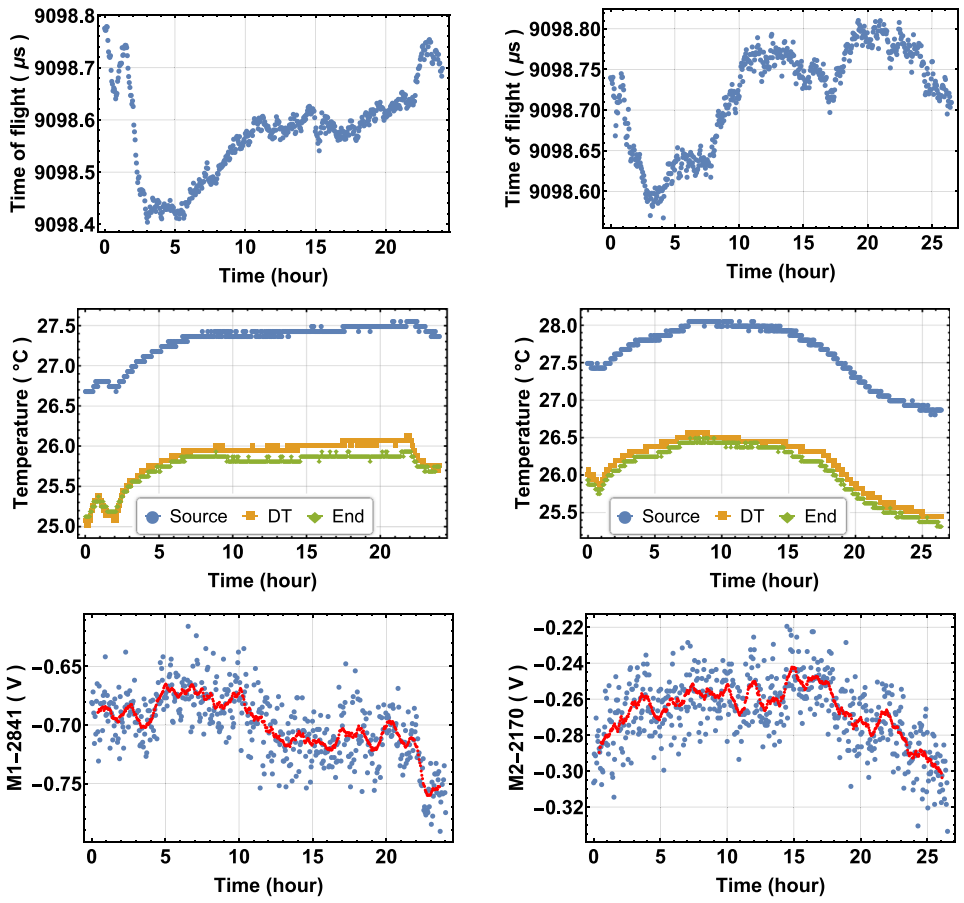

Fig. 10. The left panel is the fluctuation of the time-of-flight (top), temperature (middle), M1 voltage and 19 point moving average (bottom) as a function of time for a day-long monitoring. The right panel is the fluctuation of time-of-flight (top), temperature (middle), M2 voltage and 19 point moving average (bottom) as a function of time for a day-long monitoring.

4.2.3. Power supply influence on the width of the time-of-flight spectra

Besides the variation trend in the voltage plots in Fig. 10, there are also quicker voltage fluctuations. This fluctuation would result in a spread of the time-of-flight spectra, contributing to its width. To probe the fluctuation, after taking a 19 point moving average of the voltage (see the bottom panels in Fig. 10), we first calculated the residuals by subtracting the 19 point moving average from the voltage. Then we calculated the standard deviation of the residuals σ_V'', as a measure of how much the voltage of a given electrode is fluctuating. The results are listed in Table 1. It should be noted that the observed values for σ_V' and σ_V'' are within the ripple, noise and stability specifications of the ISEG positive and negative high precision EHS 82 60 MPOD power supplies [14] used. Then we multiplied the slope and the fluctuation standard deviation for a given electrode and added the products σ_{spec}' in quadrature, resulting in a 23 ns spread. Hence, fluctuation in the electrode potential (except for the lens) contributes approximately 23 ns to the standard deviation of the peak distribution σ_{spec}, which is typically 57 ns. The rest of the spread would come from other sources including the time base error of the pulse generator and not having a perfectly optimized tune. Once these issues are resolved, the 23 ns spread in the time-of-flight spectra stemming from the power supply voltage fluctuation indicates that we can ultimately achieve a mass resolving power above 83,000 at 400 loops or 9 ms capture time. This is consistent with the best resolving power of 70,000 we have obtained and also shows our resolving power is currently limited by the power supply stability.

5. Summary

The MR-TOF has been successfully commissioned with a resolving power of 70,000 and an efficiency of 10%. There are indications that this resolving power is limited by the power supply stability. For the on-line commissioning and operation, RC filtering will be added to the output of the power supplies to achieve greater temporal stability [15] and the pulse generator will be referenced to a more precise clock. The resolving power will be improved and be comparable to similar devices in operation and sufficient to resolve most isobars that would be produced at the N = 126 factory.

CRediT authorship contribution statement

B. Liu: Investigation, Data curation, Formal analysis, Software, Writing - original draft. **M. Brodeur:** Supervision, Investigation, Methodology, Writing - review & editing, Funding acquisition. **D.P. Burdette:** Investigation, Writing - review & editing. **J.M. Kelly:** Investigation, Software. **T. Kim:** Investigation. **J. Long:** Investigation, Writing - review & editing. **P.D. O'Malley:** Investigation, Writing - review & editing.

Declaration of competing interest

The authors declare that they have no known competing financial interests or personal relationships that could have appeared to influence the work reported in this paper.

Acknowledgment

We would like to acknowledge D. Ray for providing the CARIBU MR-TOF optimal mirror potential that served as starting point for our latest optimization, A.A. Valverde and D. Santiago for providing the

design of the CARIBU MR-TOF high-precision voltage read out box, J. Brandon for assembling the fast switch used for the BNG, and J. Kaiser for putting together the DT fast switch. We also acknowledge the help of E. Stech with our LabVIEW code, as well as T. Brunner for providing his LabVIEW code as starting point. We would like to thank P. Schury and P. Delahaye for fruitful discussion. This work was conducted with the support of the National Science Foundation under Grant Number PHY-1713857, and of the University of Notre Dame.

References

[1] M. Arnould, et al., The r-process of stellar nucleosynthesis: Astrophysics and nuclear physics achievements and mysteries, Phys. Rep. 450 (2007) 97.
[2] M. Mumpower, et al., The impact of individual nuclear properties on r-process nucleosynthesis, Prog. Part. Nucl. Phys. 86 (2016) 86.
[3] G. Savard, et al., The N = 126 factory: A new facility to produce very heavy neutron-rich isotopes, Nucl. Instrum. Methods Phys. Res. B 463 (2020) 258.
[4] J.M. Kelly, et al., First off-line tests and performance of the Notre Dame multi-reflection time-of-flight mass spectrometer, Nucl. Instrum. Methods Phys. Res. B 463 (2020) 485.
[5] B.E. Schultz, et al., Construction and simulation of a multi-reflection time-of-flight mass spectrometer at the University of Notre Dame, Nucl. Instrum. Methods Phys. Res. B 376 (2016) 251.
[6] HeatWave Labs, 2020, available at https://www.cathode.com/ (accessed on July 31st, 2020).
[7] T. Brunner, et al., A large Bradbury Nielsen ion gate with flexible wire spacing based on photo-etched stainless steel grids and its characterization applying symmetric and asymmetric potentials, Int. J. Mass Spectrom. 309 (2012) 97.
[8] R.N. Wolf, et al., Static-mirror ion capture and time focusing for electrostatic ion-beam traps and multi-reflection time-of-flight mass analyzers by use of an in-trap potential lift, Int. J. Mass Spectrom. 313 (2012) 8.
[9] Stanford Research System, DG535 digital delay/pulse generator, 2020, available at https://www.thinksrs.com/products/dg535.html (accessed on August 29th, 2020).
[10] Stanford Research System, SR430 multichannel scaler/averager, 2020, available at https://www.thinksrs.com/downloads/pdfs/manuals/SR430m.pdf (accessed on August 29th, 2020).
[11] S. Purushothaman, et al., Hyper-EMG: A new probability distribution function composed of Exponentially Modified Gaussian distributions to analyze asymmetric peak shapes in high-resolution time-of-flight mass spectrometry, Int. J. Mass Spectrom. 421 (2017) 245.
[12] CADDOCK, Type USVD and type HVD ultra-precision voltage dividers-450 Volts to 5 KV, 2020, available at http://www.caddock.com/Online_catalog/Mrktg_Lit/TypeUSVD_HVD.pdf (accessed on August 29th, 2020).
[13] DS18B20 digital thermometer, 2020, available at https://datasheets.maximintegrated.com/en/ds/DS18B20.pdf (accessed on August 29th, 2020).
[14] ISEG, EHS, 2020, available at https://iseg-hv.com/en/products/detail/EHS (accessed on August 29th, 2020).
[15] P. Schury, et al., High-stability, high-voltage power supplies for use with multi-reflection time-of-flight mass spectrographs, Rev. Sci. Instrum. 91 (2020) 014702.